

Piezotronic Effects on the Optical Properties of ZnO Nanowires

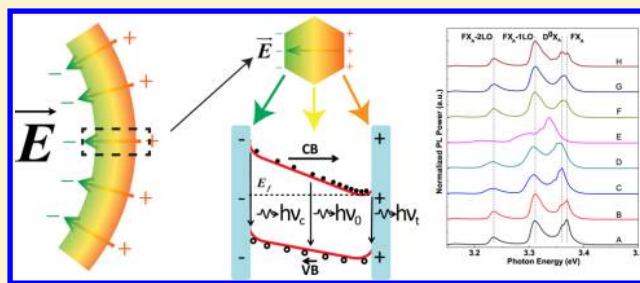
Shuigang Xu, Wenhao Guo, Shengwang Du, M. M. T. Loy, and Ning Wang*

Department of Physics and the William Mong Institute of Nano Science and Technology, The Hong Kong University of Science and Technology, Hong Kong

S Supporting Information

ABSTRACT: We report the piezotronic effects on the photoluminescence (PL) properties of bent ZnO nanowires (NWs). We find that the piezoelectric field largely modifies the spatial distribution of the photoexcited carriers in a bent ZnO NW. This effect, together with strain-induced changes in the energy band structure due to the piezoresistive effects, results in a net redshift of free exciton PL emission from a bent ZnO NW. At the large-size limit, this net redshift depends only on the strain parameter, but it is size-dependent if the diameter of the NW is comparable to that of the depletion layer. The experimental data obtained using the near-field scanning optical microscopy technique at low temperatures support our theoretical model.

KEYWORDS: ZnO nanowires, strain, bending, photoluminescence, piezotronic effects



ZnO nanowires (NWs) have attracted intense research interest due to their potential applications in field-effect transistors,^{1,2} ultraviolet lasers,³ light-emitting diodes,⁴ piezoelectric nanogenerators,^{5–7} and solar cells⁸ owing to ZnO's wide direct bandgap (3.37 eV) and large exciton binding energy (60 meV).⁸ When fabricating nano structures and devices using ZnO NWs, strain is unavoidable and often modifies the NW's mechanical,⁹ electronic,^{10,11} and optical properties.^{12,13} Some studies have revealed that strain can induce a significant redshift and broadening of the near-band-edge (NBE) emission in the cathodoluminescence (CL) spectra of a bent ZnO NW.¹⁴ Most recently, Wei et al. reported the size-dependent shift of the NBE peak, but a conclusive interpretation of bandgap modulation was not possible with their room-temperature CL data.¹⁵ Using high-resolution low-temperature CL spectroscopy, Han et al. were able to further resolve the shift of the free exciton (FX) line and attribute the overall redshift to the strain-gradient effect.¹⁶

In this work, we find that the net redshift of FX photoluminescence (PL) emission in a bent ZnO NW is mainly caused by strain-induced changes in the energy band structure together with the piezotronic effects, which modifies the spatial local distribution of photoexcited carriers. At the large-size limit, this net redshift depends only on the strain parameter, but it is size-dependent if the diameter of the NW is comparable to that of the depletion layer. The experimental results measured using near-field scanning optical microscopy (NSOM) techniques at a low temperature (90 K) support our theoretical model, which fully reveals the microscopic origin of the strain effects in ZnO NWs for all of the previous experiments.^{14–16} A further study of the phonon–exciton interaction shows that the strain in bent ZnO NWs can also

induce phonon energy variations besides the change in the bandgap and the piezotronic effects.

ZnO produces the piezotronic effects when it is strained.¹⁷ For a bent ZnO NW, tensile strain and compressive strain occur at the outer and inner surfaces, respectively.⁵ Positive and negative charges (static and nonmobile) are therefore generated on these surfaces which cannot be recombined without releasing the strain. An electric field across the cross section of a *c*-axis-oriented ZnO NW is then built up as shown in Figure 1a. Figure 1b shows the energy band diagrams for a straight ZnO NW. When the NW is excited by photons with energy larger than the bandgap, electron–hole pairs are

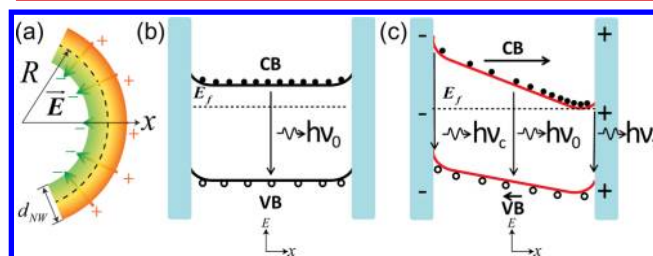


Figure 1. (a) Schematic diagrams of bending induced piezotronic effects. (b) The energy band diagram of an unbent NW. The bandgap is homogeneous across the cross section. The band edges are bent upward near the surface owing to the surface Fermi-level pinning. (c) The case for a bent NW. The deformation induces the inhomogeneous bandgap, while the piezoelectric field modulates the spatial distribution of photocarriers.

Received: August 23, 2012
Revised: October 5, 2012
Published: October 11, 2012

generated. These excitons then recombine and emit photons with energy ($h\nu_0$) approximately equal to the bandgap of ZnO. When we collect all of the photons emitted from the ZnO NW, the corresponding peak in the PL appears exactly at the position with a photon energy of $h\nu_0$. It has been reported that oxygen molecules are always adsorbed on ZnO surfaces and capture the free electrons in ZnO which is n-type by nature.¹⁸ Therefore low conductive depletion layers form near the surfaces. The depletion layers result in upward bending for both conduction and valence bands at the surfaces of ZnO NWs. However, the surface potential cannot disrupt the homogeneous distribution of the bandgap. In the PL spectrum of ZnO, the NBE emission is actually due to the contribution of several emissions such as the FX, FX phonon replicas, and the bound exciton (BX), which can be distinguished by measurement at low temperatures.^{19,20}

Figure 1c shows the inhomogeneous bandgap and charge carrier distribution across the cross section of a bent ZnO NW. The bandgap of ZnO decreases under a tensile (c -axis) strain and increases under a compressive (c -axis) strain.¹⁴ Therefore, the photons emitted from the outer surface of a bent ZnO NW have a smaller photon energy ($h\nu_t < h\nu_0$), whereas the photons emitted from the inner surface have a larger photon energy ($h\nu_c > h\nu_0$) than that emitted from the strain-free neutral axis ($h\nu_0$). Note that the change in the bandgap discussed above known as the piezoresistive effects is a common feature of all semiconductors and is not limited to ZnO. On the other hand, for the wurtzite ZnO structure, the piezotronic effects are not negligible because of the polarization of ions in ZnO (noncentral symmetry).²¹ Under the piezoelectric field, the photoexcited electrons will drift toward and aggregate at the NW outer surface.²² Although the holes will drift toward the inner surface under the same electric field, the density of holes at the outer surface is still considerably high under the steady excitation of the laser source. Moreover, the mobility of holes is much smaller than that of electrons, and the carrier recombination lifetime is extremely short in ZnO.²³ For a NW with a diameter of 900 nm, the transit time for holes from outer to inner surface is found to be on the order of 13.5 ns (based on the hole mobility μ of $2 \text{ cm}^2/\text{V s}$,²⁴ the piezoelectric potential of 0.3 V^{25}), which is much larger than the carrier recombination lifetime of ZnO ($\sim 0.86 \text{ ns}^{26}$), while the transit time of electrons (the electron mobility $\sim 115 \text{ cm}^2/\text{V s}^{27}$) is about 0.235 ns, smaller than the lifetime. Therefore, on the scale of the carrier recombination lifetime, it is reasonable to believe that the concentration of holes in this case is negligibly affected by the piezoelectric field. Since ZnO is a direct bandgap semiconductor, the recombination rate is proportional to the electron and hole concentrations. As a result, the number of photons emitted from the outer surface of the NW (with photon energy $h\nu_t$) is much larger than that from the inner surface. If we collect all of the photons emitted from the entire cross section, the related emission peak in the PL will move to the position with photon energy $h\nu_b$ that is, a net redshift of the FX in the PL of bent ZnO NWs because of the piezoelectric field.

We develop a quantitative model to estimate the strain-induced redshift (under the piezoelectric field) in the bent NW. Under the steady-state laser excitation, the electron density in the NW follows the Boltzmann distribution

$$n(x) = n_c \exp\left(-\frac{E_c(x)}{kT}\right) \quad (1)$$

where n_c is a constant determined by the laser intensity, k the Boltzmann constant, T the absolute temperature, and $E_c(x)$ the conduction band edge as a function of spatial coordinate. Under the strain-induced piezoelectric field and deformation, $E_c(x)$ becomes

$$\begin{aligned} E_c(x) &= E_{c_0}(x) + \Delta E_c(x) \\ &= E_{c_0}(x) + \Delta E_c^{\text{piezo}}(x) + \Delta E_c^{\text{deform}}(x) \end{aligned} \quad (2)$$

where $E_{c_0}(x)$ is the conduction band edge of a strain free NW, $\Delta E_c^{\text{piezo}}(x)$ the band edge shift due to the piezoelectric potential, and $\Delta E_c^{\text{deform}}(x)$ the band edge shift due to the deformation potential. For the piezoelectric potential, we take the first order approximation²⁵ and define $b = \partial \Delta E_c^{\text{piezo}} / \partial \epsilon$. In the bent NW, because the strain varies approximately linearly across the NW cross section,²⁸ we write down the piezoelectric potential as

$$\Delta E_c^{\text{piezo}}(x) = -\frac{2b\epsilon_c^{\text{max}}x}{d_{\text{NW}}} \quad (3)$$

where ϵ_c^{max} is the local maximum strain and d_{NW} the diameter of NW. The deformation potential comes from the strain induced bandgap change, which can be described by the deformation potential constant:²⁹ $\partial E_g / \partial \epsilon = a_g$. The conduction band edge modified by the deformation potential is then

$$\Delta E_c^{\text{deform}}(x) = \frac{\epsilon_c^{\text{max}}a_gx}{d_{\text{NW}}} \quad (4)$$

According to Figure 1b, $\Delta E_{c_0}(x)$ of the strain-free NW is not uniform across the cross section because of the surface depletion. In a ZnO NW, the surface depletion region is estimated as³⁰ $W = [2\epsilon_{\text{ZnO}}\phi_s / (eN_D)]^{1/2}$, where ϵ_{ZnO} is the dielectric constant of ZnO, ϕ_s the surface potential ($\sim 0.5 \text{ eV}$), e the electron charge, and N_D the doping density. We can crudely modify E_{c_0} by this surface potential using a parabolic shape.

Since the recombination rate of charge carriers is proportional to the electron concentration, the PL spectrum acquired from the bent cross section is given by

$$I(h\nu) = A \int n(x)f[h\nu - h\nu_c(x)]dx \quad (5)$$

where $f(h\nu - h\nu_c)$ is the Lorentzian line shape from a point source and A a constant. Because the piezoelectric field does not affect the local bandgap, the position-dependent photon central energy can be obtained as $h\nu_c(x) = E_g + 2\Delta E_c^{\text{deform}}(x)$, where E_g is the bandgap of a strain-free NW. Equation 5 determines the PL spectrum. If the depletion layer can be ignored (i.e., $d_{\text{NW}} \gg W$), eq 5 can be simplified to

$$I(h\nu) = Ad_{\text{NW}}I_t(h\nu)/\epsilon_c^{\text{max}} \quad (6)$$

where $I_t(h\nu)$ is independent of the diameter (please see the details in Supporting Information). So the PL spectrum profile is independent of the NW diameter. The diameter only affects the intensity of PL.

To confirm our analysis, we first investigated the strain effect in bent ZnO NWs at the atomic scale by high-resolution transmission electron microscopy (HRTEM). The ZnO NWs used here were synthesized via chemical vapor deposition.^{31,32} The individual bent NWs were transferred to a carbon holey supporting film with a tangential force using the physical dry transfer method.³³ The large aspect ratio and elastic flexibility

of as-grown ZnO NWs allowed this bending process. To study the bending effect on the optical properties of ZnO NWs, we carried out measurement of spatially resolved PL on individual ZnO NWs at low temperatures using NSOM. The ZnO NWs were first dispersed on a silicon substrate. Then a single ZnO NW was bent by a micromanipulator tipped with a sharp tungsten probe under an optical microscope. After bending, the strong van der Waals interaction between the NWs and the substrate kept the NWs bent. Spatially resolved PL measurements were performed using the NSOM setup (Nanonics CryoView2000 equipped with a 325 nm He–Cd laser source via a tip probe which has a 500 nm aperture at liquid nitrogen temperature 90 K). The setup is illustrated in Figure 2. The

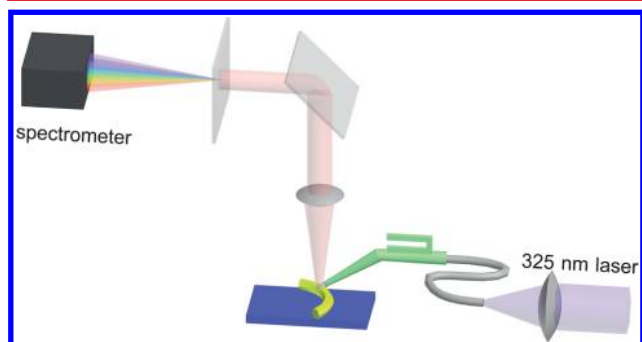


Figure 2. Schematic illustration of the PL measurements for bent NWs by NSOM.

spot size was set to 3 μm by adjusting the distance between the tip and the samples, ensuring that all photons emitted from the local area were collected. The luminescence was detected by a spectrometer (QE65000, Ocean Optics) with a resolution of 0.09 nm. After the low-temperature PL measurements on the bent ZnO NWs, we added a drop of ethanol on to the substrate which caused the NWs to unbend and straighten up again.

Figure 3a shows the typical TEM image of a bent ZnO NW. This bent NW had a uniform diameter of 52 nm. Figure 3b shows the selected-area electron diffraction (SAED) at the position labeled “c” in Figure 3a. The SAED pattern indicates that the NW grew along the [0001] direction (*c*-axis). Figure 3c and d are HRTEM images of the straight and bent portions of the NW (labeled by “c” and “d” in Figure 3a, respectively). The HRTEM images of the outer (Figure 3e), center (Figure 3f), and inner (Figure 3g) parts of the straight portion(s) show that the lattice constants along the *c*-axis are uniform, that is, $c_0 = 0.514$ nm when there is no strain. But at the bent portion(s), the tensile strain increases the lattice constant to $c_{\text{outer}} = 0.519$ nm, whereas the compressive strain decreases it to $c_{\text{inner}} = 0.508$ nm. The strain-free neutral axis has a similar lattice constant as the straight part. Since no defects are observed in the bent NW, the variations in the lattice constants should be attributed to the elastic bending deformation. The maximum tensile strain and compressive strain can be quantitatively calculated by

$$\epsilon_c^{\text{max}} = \left| \frac{c_{\text{outer}} - c_0}{c_0} \right| = \left| \frac{c_{\text{inner}} - c_0}{c_0} \right| \quad (7)$$

Then, we can estimate the maximum tensile strain (about 1.0%) and the maximum compressive strain (about 1.2%). Obviously, the strain in the bent NW varies linearly from tension to compression across the NW. The linear strain indicated the linear bandgap distribution in the bent NW,

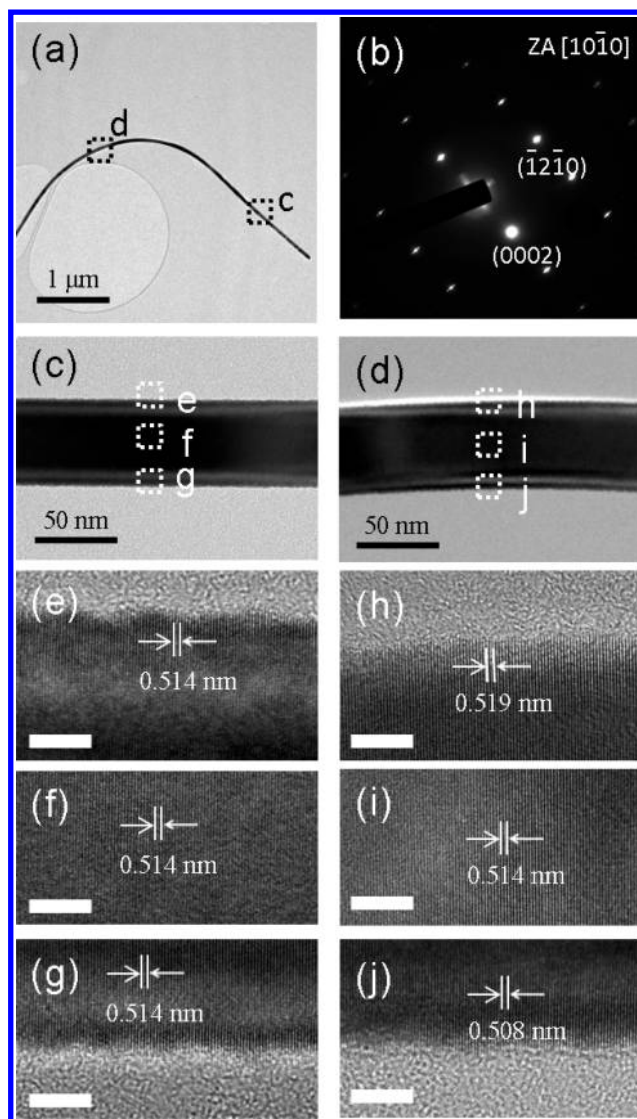


Figure 3. TEM images of a bent ZnO NW. (a) Low magnification image of the NW. (b) SAED taken from position “c” in part a indicating [0001] growth direction of the ZnO NW. (c) The straight region (labeled by “c” in a) of the NW. The HRTEM images taken from the outer, center, and inner of the NW in this straight region are shown in figures e, f, and g, respectively. The lattice constant *c* is quite uniform. (d) The bent region (labeled by “d” in a). The HRTEM images taken from the outer, center, and inner of the NW in this bent region are shown in figures h, i, and j, respectively. The lattice constant *c* increases in the tensile side and decreases in the compressive side. The scale bars in e–j are 5 nm.

because the theoretical calculations revealed that the electronic bandgap for ZnO NWs with large enough diameters was inversely proportional to strain and showed a linear relationship.³⁴ However, this strain estimation is impractical because the HRTEM measurement is made ex situ with respect to the PL system. Fortunately, we can calculate the maximum tensile or compressive strain by³³

$$\epsilon_c^{\text{max}} = \frac{d_{\text{NW}}}{2R} \quad (8)$$

where d_{NW} is the diameter of the NW and *R* the local radius of the curvature. By this way, the calculated strain in the NW shown in Figure 3d is about 1.2%, which agrees well with that

(1.0% or 1.2%) from the HRTEM results. In the following discussions, we follow eq 8 to determine the local maximum strain in the bent region.

The PL spectra of a typical bent ZnO NW with a diameter of 900 nm are shown in Figure 4a. The low-temperature PL

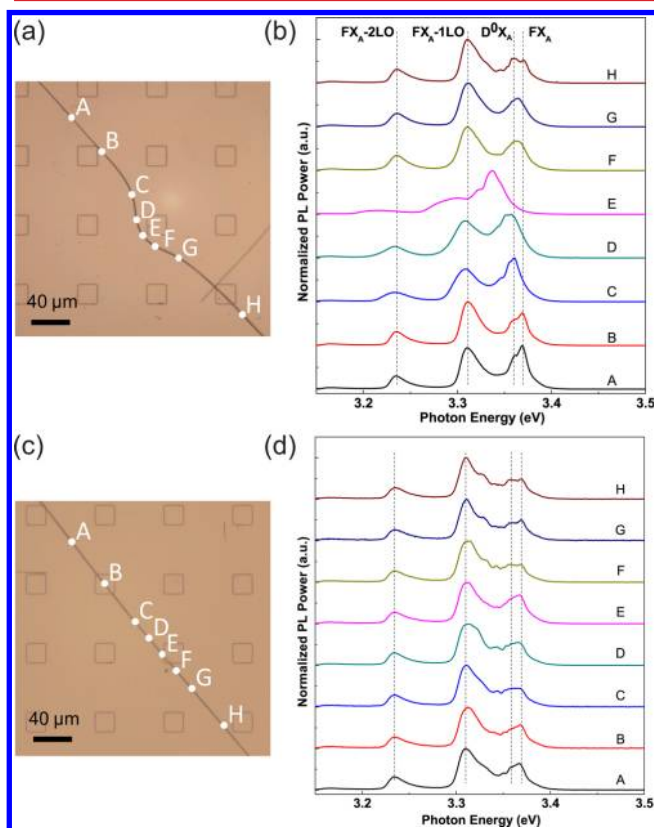


Figure 4. (a) The optical image of the bent ZnO NW. (b) The corresponding PL spectra taken from each arrowed positions in a. (c) The optical image of the same NW after releasing the deformation. (d) The PL spectra of straight NW at different positions labeled in c. The NW has a diameter of 900 nm.

spectra acquired from different bending curvatures as indicated by A–H are shown in Figure 4b. The peak center of each emission can be determined by fitting the spectra using Lorentzian line shape function. Apparently, at the strain free region, we can observe four prominent peaks at the NBE region: the free exciton (FX_A) at 3.370 eV, the neutral-donor-bound exciton (D^0X_A) at 3.361 eV, the first-order longitudinal optical phonon replica of the free exciton (FX_A-1LO) at 3.311 eV, and the second-order longitudinal optical phonon replica of the free exciton (FX_A-2LO) at 3.235 eV. A significant redshift of FX_A can be clearly observed at the bent regions. The shift increases with increasing the local bent curvature, and this agrees well with our previous analysis. It is necessary to emphasize that the bending deformation of the ZnO NW here is elastic because this NW can recover to its straight shape (see Figure 4c) when we add a drop of ethanol to the substrate. In this case, all of these peaks in the PL shift back to the original positions of straight NW.

The redshift of the free exciton which depends on the local maximum strain in the bent region is depicted in Figure 5a. Obviously, the magnitude of the redshift increased linearly with increasing the local maximum strain. The red solid line, numerically obtained from eqs 1–5 with fitting parameters $b =$

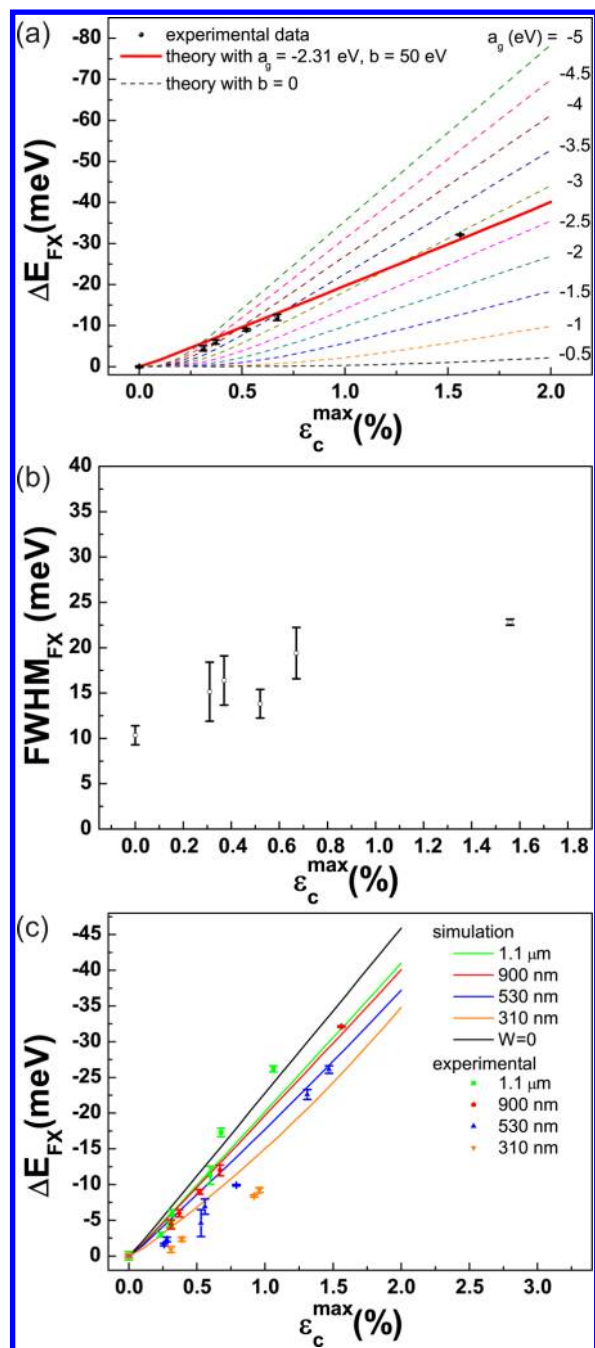


Figure 5. Energy shift and FWHM of the FX_A emission versus the local maximum strain ϵ_c^{\max} in bent NWs. (a) Comparison between the experimental data and simulation results. The scatters are for the experimental data from the 900 nm NW. The solid line is the numerical results considering both the strain-induced piezoelectric field ($b = 50$ eV) and the deformation potential ($a_g = -2.31$ eV) in the bent ZnO NW. The dashed lines are the numerical results for different a_g without accounting the piezoelectric effect ($b = 0$). (b) FWHM of FX_A versus ϵ_c^{\max} . (c) Comparison between the experimental data and simulation results for the NWs with different diameters. The slight difference for different diameters both in experimental data and simulation results is due to the surface depletion. Here the simulation result obtained by assuming the depletion layer $W = 0$ is also given for comparison.

50 eV and $a_g = -2.31$ eV, agrees very well with the experimental data. For comparison, we also plot the numerical curves (dashed lines) of the redshift without accounting for the

piezotronic effects. It is clear that, even if we vary the parameter of a_g in a large range (but with $b = 0$), the strain-dependent redshift cannot be fully explained by the NW deformation. This further confirmed that the piezoelectric field plays an important role in the optical properties of the bent ZnO NW. In fact, the deformation potential, which spatially modulates the central energy of emitted photons, on the other hand, plays a negligible role in determining the spatial electron density distribution as compared with the piezoelectric potential.²² The variation of full-width at half-maximum (FWHM) of the FX_A under different strain is plotted in Figure 5b. Considering the error, the strain effect on FWHM is not as pronounced as that on the shift. The slightly broadening of FX_A under large strain indicates the exist of piezoresistive effects.

We have also investigated how the NW diameter influences the strain-induced redshift of free exciton. If the surface depletion is not taken into account, the curve of ΔE_{FX_A} versus ϵ_c^{\max} is not dependent on the diameter of the NWs (see details in Supporting Information). In reality, in addition to the piezoelectric potential, both the high surface potential (~ 0.5 eV) and the wide depletion layer (~ 71 nm) affect the distribution of electrons. Figure 5c shows the experimental data and calculation results of the strain effect for different NW diameters. We can see that the slopes of ΔE_{FX_A} as a function of ϵ_c^{\max} slightly decrease with the decreasing of diameters. The experimental data also shows a similar trend and confirm that the strain-induced redshift is not sensitive to the NW diameter as $d_{NW} \gg W$.

It should be emphasized that, with sufficiently high spatial resolution, in principle the strain induced redshift of FX_A in the tensile region and the blueshift in the compressive region of the NW can be distinguishable.¹⁶ However, the exciton in ZnO NWs can diffuse. The diffusion length of the exciton is up to ~ 110 nm.¹⁴ This means that the acquired spectra are always the integral of the emissions from tensile and compressive regions even the exciting spot is very small. Therefore, we should observe the redshift even we excite the region of the neutral axis of the NW because of the inhomogeneous distribution of the charge carries. Due to the aggregation of electrons in the tensile region, the intensity of the PL emission from this region is larger than that from the compressive region.¹⁶ If there is no piezoelectric field in the NWs, the tensile-strain-induced redshift and compressive-strain-induced blueshift will equally contribute to the NBE emission, resulting in broadening of the NBE peak. A similar feature has been observed in the Raman spectra of InP bent NWs.³⁵

By examining the spectra shown in Figure 4b carefully, one can identify the redshifts not only for the FX_A , but also for D^0X_A , FX_A -1LO, and FX_A -2LO peaks. The shifts of FX_A -1LO and FX_A -2LO, which are related to the LO phonon–exciton interaction, are not obvious. Figure 6 summarizes the redshifts of all four emissions under different strain states. The linear fittings to the experimental data yield $\partial E_{FX_A}/\partial \epsilon_c^{\max} = -1.97$ eV, $\partial E_{D^0X_A}/\partial \epsilon_c^{\max} = -2.08$ eV, $\partial E_{FX_A-1LO}/\partial \epsilon_c^{\max} = -0.60$ eV, and $\partial E_{FX_A-2LO}/\partial \epsilon_c^{\max} = -0.13$ eV. Obviously, $\partial E_{D^0X_A}/\partial \epsilon_c^{\max}$ is approximately equal to $\partial E_{FX_A}/\partial \epsilon_c^{\max}$, indicating that the mechanism of the strain effect on D^0X_A is similar to that on FX_A . However, the $\partial E_{FX_A-1LO}/\partial \epsilon_c^{\max}$ and $\partial E_{FX_A-2LO}/\partial \epsilon_c^{\max}$ show many different features. This indicates that the strain effect affects not only the band structure of ZnO NWs but also the phonon–exciton interaction. For the exciton–phonon cou-

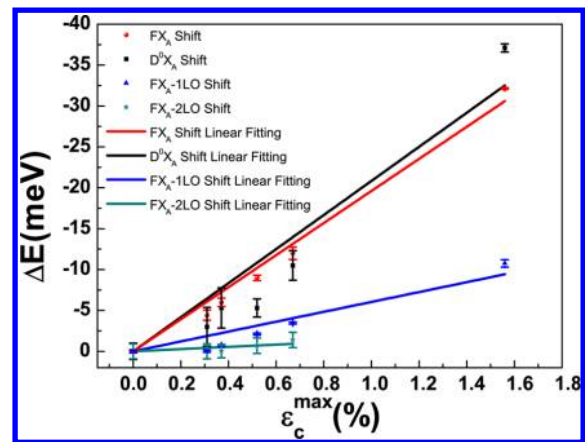


Figure 6. Energy shifts of FX_A , D^0X_A , FX_A -1LO, and FX_A -2LO versus the local maximum strain. The scatters are obtained from PL spectra of the bent ZnO NW (900 nm in diameter). The solid lines are the linear fitting results.

pling, the FX_A and its LO-phonon replicas can be described by³⁶

$$E_{FX_A-mLO} = E_{FX_A} - m\hbar\omega_{LO} + \left(L + \frac{1}{2}\right)kT \quad (9)$$

$(m = 1, 2)$

where $m\hbar\omega_{LO}$ is the LO-phonon energy (72 meV when there is no strain), $(L + 1/2)$ is related to the kinetic energy of the exciton ($L = 1$ for 1-LO replicas and $L = 0$ for 2-LO replicas). From eq 9, if we add the strain effect, we can get

$$\frac{\partial \Delta E_{FX_A-mLO}}{\partial \epsilon_c^{\max}} = \frac{\partial \Delta E_{FX_A}}{\partial \epsilon_c^{\max}} - m \frac{\partial \Delta \hbar\omega_{LO}}{\partial \epsilon_c^{\max}} \quad (10)$$

From our experimental results ($\partial \Delta E_{FX_A-mLO}/\partial \epsilon_c^{\max} \neq \partial \Delta E_{FX_A}/\partial \epsilon_c^{\max}$), we can conclude that the strain can change the phonon energy ($\partial \Delta \hbar\omega_{LO}/\partial \epsilon_c^{\max} \neq 0$). From Figure 6, we can figure out the average of $\partial \Delta \hbar\omega_{LO}/\partial \epsilon_c^{\max}$ to be -1.15 eV.

It is reasonable to suggest that strain can influence lattice vibrations and thus result in phonon energy variations which can be revealed using Raman spectroscopy techniques.^{35,37,38} For bent ZnO NWs, Figure S2 (see Supporting Information) shows that the phonon peak in the Raman spectrum is sensitive to strain. In particular, tensile strain and compressive strain shifted the phonon peak to positions with lower and higher wavenumbers, respectively.

In summary, we have demonstrated that the piezoelectric field in bent ZnO NWs modulates the distribution of photocarriers. The piezotronic effects, together with the inhomogeneous bandgap across the cross section of ZnO NWs, result in the redshift of FX_A in bent ZnO NWs. The redshift is found to be linearly proportional to ϵ_c^{\max} and slightly influenced by the NW diameter, as our numerical calculation has shown. Furthermore, the bending-induced variations in phonon energy are presented by the minor redshift of FX -mLO.

■ ASSOCIATED CONTENT

📄 Supporting Information

Material about low-temperature PL spectra of a bent ZnO nanowire with a diameter of about 310 nm, details of energy shift versus diameter of the NWs, and Raman spectroscopy of

bent ZnO nanowires. This material is available free of charge via the Internet at <http://pubs.acs.org/>.

AUTHOR INFORMATION

Corresponding Author

*E-mail: phwang@ust.hk

Notes

The authors declare no competing financial interest.

ACKNOWLEDGMENTS

The authors are grateful for fruitful discussions with Professor J. N. Wang (Physics, the Hong Kong University of Science and Technology) and Professor W. L. Guo (Nanjing University of Aeronautics and Astronautics, P. R. China). Financial support from the Research Grants Council of Hong Kong (Project Nos. CityUS/CRF/08, 604009, 603408) and technical support of the Raith-HKUST Nanotechnology Laboratory for the electron-beam lithography facility at MCPF (Project No. SEG_HKUST08) are hereby acknowledged.

REFERENCES

- (1) Fan, Z. Y.; Wang, D. W.; Chang, P. C.; Tseng, W. Y.; Lu, J. G. *Appl. Phys. Lett.* **2004**, *85*, 5923–5925.
- (2) Goldberger, J.; Sirbully, D. J.; Law, M.; Yang, P. *J. Phys. Chem. B* **2005**, *109*, 9–14.
- (3) Chu, S.; Wang, G. P.; Zhou, W. H.; Lin, Y. Q.; Chernyak, L.; Zhao, J. Z.; Kong, J. Y.; Li, L.; Ren, J. J.; Liu, J. L. *Nat. Nanotechnol.* **2011**, *6*, 506–510.
- (4) Bie, Y. Q.; Liao, Z. M.; Wang, P. W.; Zhou, Y. B.; Han, X. B.; Ye, Y.; Zhao, Q.; Wu, X. S.; Dai, L.; Xu, J.; Sang, L. W.; Deng, J. J.; Laurent, K.; Leprince-Wang, Y.; Yu, D. P. *Adv. Mater.* **2010**, *22*, 4284–4287.
- (5) Wang, Z. L.; Song, J. H. *Science* **2006**, *312*, 242–246.
- (6) Wang, Z. L. *MRS Bull.* **2012**, *37*, 814–827.
- (7) Wang, Z. L. *Adv. Mater.* **2012**, *24*, 4632–4646.
- (8) Law, M.; Greene, L. E.; Johnson, J. C.; Saykally, R.; Yang, P. D. *Nat. Mater.* **2005**, *4*, 455–459.
- (9) Zheng, K.; Han, X. D.; Wang, L. H.; Zhang, Y. F.; Yue, Y. H.; Qin, Y.; Zhang, X. N.; Zhang, Z. *Nano Lett.* **2009**, *9*, 2471–2476.
- (10) Kwon, S. S.; Hong, W. K.; Jo, G.; Maeng, J.; Kim, T. W.; Song, S.; Lee, T. *Adv. Mater.* **2008**, *20*, 4557–4562.
- (11) Zhang, Y.; Liu, Y.; Wang, Z. L. *Adv. Mater.* **2011**, *23*, 3004–3013.
- (12) Yang, Q.; Wang, W. H.; Xu, S.; Wang, Z. L. *Nano Lett.* **2011**, *11*, 4012–4017.
- (13) Dietrich, C. P.; Lange, M.; Klupfel, F. J.; von Wenckstern, H.; Schmidt-Grund, R.; Grundmann, M. *Appl. Phys. Lett.* **2011**, *98*, 031105.
- (14) Han, X. B.; Kou, L. Z.; Lang, X. L.; Xia, J. B.; Wang, N.; Qin, R.; Lu, J.; Xu, J.; Liao, Z. M.; Zhang, X. Z.; Shan, X. D.; Song, X. F.; Gao, J. Y.; Guo, W. L.; Yu, D. P. *Adv. Mater.* **2009**, *21*, 4937–4941.
- (15) Wei, B.; Zheng, K.; Ji, Y.; Zhang, Y.; Zhang, Z.; Han, X. *Nano Lett.* **2012**, *12*, 4595–4599.
- (16) Han, X.; Kou, L.; Zhang, Z.; Zhang, Z.; Zhu, X.; Xu, J.; Liao, Z.; Guo, W.; Yu, D. *Adv. Mater.* **2012**, *24*, 4707–4711.
- (17) Wang, Z. L. *Adv. Mater.* **2007**, *19*, 889–892.
- (18) Gao, P.; Wang, Z. Z.; Liu, K. H.; Xu, Z.; Wang, W. L.; Bai, X. D.; Wang, E. G. *J. Mater. Chem.* **2009**, *19*, 1002–1005.
- (19) Ozgur, U.; Alivov, Y. I.; Liu, C.; Teke, A.; Reshchikov, M. A.; Dogan, S.; Avrutin, V.; Cho, S. J.; Morkoc, H. *J. Appl. Phys.* **2005**, *98*, 041301.
- (20) Feng, L.; Cheng, C.; Yao, B. D.; Wang, N.; Loy, M. M. T. *Appl. Phys. Lett.* **2009**, *95*, 053113.
- (21) Wang, Z. L. *J. Phys. Chem. Lett.* **2010**, *1*, 1388–1393.
- (22) Gao, Y.; Wang, Z. L. *Nano Lett.* **2009**, *9*, 1103–1110.
- (23) Ma, X. Y.; Chen, P. L.; Li, D. S.; Zhang, Y. Y.; Yang, D. R. *Appl. Phys. Lett.* **2007**, *91*, 021105.
- (24) Look, D. C.; Reynolds, D. C.; Litton, C. W.; Jones, R. L.; Eason, D. B.; Cantwell, G. *Appl. Phys. Lett.* **2002**, *81*, 1830–1832.
- (25) Gao, Y.; Wang, Z. L. *Nano Lett.* **2007**, *7*, 2499–2505.
- (26) Teke, A.; Ozgur, U.; Dogan, S.; Gu, X.; Morkoc, H.; Nemeth, B.; Nause, J.; Everitt, H. O. *Phys. Rev. B* **2004**, *70*, 195207.
- (27) Kaidashev, E. M.; Lorenz, M.; von Wenckstern, H.; Rahm, A.; Semmelhack, H. C.; Han, K. H.; Benndorf, G.; Bundesmann, C.; Hochmuth, H.; Grundmann, M. *Appl. Phys. Lett.* **2003**, *82*, 3901–3903.
- (28) Wang, L. H.; Han, X. D.; Zhang, Y. F.; Zheng, K.; Liu, P.; Zhang, Z. *Acta Mater.* **2011**, *59*, 651–657.
- (29) Shan, W.; Walukiewicz, W.; Ager, J. W.; Yu, K. M.; Zhang, Y.; Mao, S. S.; Kling, R.; Kirchner, C.; Waag, A. *Appl. Phys. Lett.* **2005**, *86*, 153117.
- (30) Liao, Z. M.; Zhang, H. Z.; Zhou, Y. B.; Xu, J.; Zhang, J. M.; Yu, D. P. *Phys. Lett. A* **2008**, *372*, 4505–4509.
- (31) Yao, B. D.; Chan, Y. F.; Wang, N. *Appl. Phys. Lett.* **2002**, *81*, 757–759.
- (32) Wang, N.; Cai, Y.; Zhang, R. Q. *Mater. Sci. Eng. Rep.* **2008**, *60*, 1–51.
- (33) Xue, H. Z.; Pan, N.; Li, M.; Wu, Y. K.; Wang, X. P.; Hou, J. G. *Nanotechnology* **2010**, *21*, 215701.
- (34) Yang, Y. R.; Yan, X. H.; Xiao, Y.; Lu, D. *Appl. Phys. Lett.* **2010**, *97*, 033106.
- (35) Chen, J. N.; Conache, G.; Pistol, M. E.; Gray, S. M.; Borgstrom, M. T.; Xu, H. X.; Xu, H. Q.; Samuelson, L.; Hakanson, U. *Nano Lett.* **2010**, *10*, 1280–1286.
- (36) Mendelsberg, R. J.; Allen, M. W.; Durbin, S. M.; Reeves, R. J. *Phys. Rev. B* **2011**, *83*, 205202.
- (37) Sahoo, S.; Sharma, G. L.; Katiyar, R. S. *J. Raman Spectrosc.* **2012**, *43*, 72–75.
- (38) Yan, B.; Chen, R.; Zhou, W. W.; Zhang, J. X.; Sun, H. D.; Gong, H.; Yu, T. *Nanotechnology* **2010**, *21*, 445706.